AIMS Mathematics, 10(3): 4558–4578.
DOI: 10.3934/math.2025211
Received: 13 September 2024
Revised: 11 December 2024
Accepted: 23 December 2024
Published: 03 March 2025

https://www.aimspress.com/journal/Math

Research article

Bifurcation analysis, chaotic behaviors, and explicit solutions for a fractional two-mode Nizhnik-Novikov-Veselov equation in mathematical physics

Noor Alam[1], Mohammad Safi Ullah[2], Jalil Manafian[3,4,*], Khaled H. Mahmoud[5], A. SA. Alsubaie[5], Hamdy M. Ahmed[6], Karim K. Ahmed[7] and Soliman Al Khatib[8]

[1] Department of Mathematics, Kishoreganj University, Kishoreganj 2300, Bangladesh
[2] Department of Mathematics, Comilla University, Cumilla-3506, Bangladesh
[3] Department of Applied Mathematics, Faculty of Mathematical Sciences, University of Tabriz, Tabriz, Iran
[4] Natural Sciences Faculty, Lankaran State University, H. Aslanov str., Lankaran, Azerbaijan
[5] Department of Physics, College of Khurma University College, Taif University, Taif 21944, Saudi Arabia
[6] Department of Mathematics and Engineering Physics, Higher Institute of Engineering, El-Shorouk Academy, El-Shorouk City, Cairo, Egypt
[7] Department of Mathematics, Faculty of Engineering, German International University (GIU), New Administrative Capital, Cairo, Egypt
[8] College of Engineering and Technology, American University in the Emirates (AUE), Academic City, P.O. Box 503000, Dubai, UAE

* **Correspondence:** Email: manafeian2@gmail.com.

Abstract: The two-mode Nizhnik-Novikov-Veselov (TMNNV) equation finds wide-ranging utility across engineering and scientific fields. It stands as a notable nonlinear physical model for explaining nonlinear soliton propagation. This study explores bifurcation analysis for the (2+1)-dimensional conformable time-fractional TMNNV model for the first time. Also, we have derived the explicit solutions of this model, and these solutions exhibit some unique dynamical patterns: combo bright-dark bell wave, periodic wave, bright soliton, and dark soliton, which are used in several optical applications. 2-D plots and combined 3-D with density plots are presented with the impacts of different

parameters. Later, phase portraits and the multistability of this dynamical model are analyzed via intersecting figures with the help of the planner dynamical system. We also examine the quasi-periodic and chaotic behaviors of the governing model under different conditions. Finally, conclusions are drawn based on the results.

Keywords: chaotic nature; bifurcation; phase portraits; multistability; equilibrium point
Mathematics Subject Classification: 35C08, 74J35

1. Introduction

Recent research has been focused more on the nonlinear time-dependent models that have been seen in different branches of science and engineering, namely, plasma physics [1], nano-fiber optics [2], magnetohydrodynamics [3], etc. There are different kinds of nonlinear fields such as the (3+1)-D Burger model [4], the Phi-four model [5], the Zoomeron system [6], the Chen-Lee-Liu equation [7], the iterated function system using interpolative Kannan operators [8], the generalized KP model [9], the KdV-burgers-Fisher equation [10], the Benjamin-Ono system [11], the Sawada-Kotera system [12], the generalized CBS-BK model [13], etc.

To solve these models, researchers use diverse analytical methods such as the Darboux transformation technique [14], the enhanced Kudryashov scheme [15], the generalized KP equation [16], the new Kudryashov's scheme [17], the fuzzy control approach [18], the Cauchy problem for matrix factorizations [19], the physics-informed neural networks approach [20], the modified alternative $\left(\frac{G'}{G}\right)$-expansion algorithm [21], $\left(\frac{G'}{G^2}\right)$ expansion method [22], the stochastic logical networks method [23], the first integral technique [24], METF technique [25], the modified extended direct algebraic method [26], Takagi-Sugeno fuzzy model approach to the nonlinear lateral dynamics [27], and many other methods [28–30].

Marwan and Jaradat obtained an innovative model named the next (2+1)-dimensional two-mode Nizhnik-Novikov-Veselov (TMNNV) equation, which represents a variety of physical processes occurring in diverse mediums, including biological membranes, optical fibers, modern strings, magnetoelectric dynamics, and inelastic fluids [31]. The nonlinear problems play a crucial role in the study of nonlinear wave propagation. The nonlinearity is prevalent across various fields of applied science, nonlinear dynamics, mathematical physics, and engineering, including biosciences, plasma physics, geochemistry, and fluid mechanics [32–34]. Nonlinear problems (NLPs) are significant equations because they are implemented for the mathematical modeling of numerous real-world applications [35,36]. In recent years, the calculus of NLPs has emerged as a prominent area of focus within nonlinear dynamics [37,38]. NLPs, which encompass more comprehensive forms of differential equations (DEs), significantly contribute to the qualitative analysis of many nonlinear wave propagation phenomena [39,40]. This work identifies bifurcation, multistability, quasi-periodic, and chaotic behavior in the fractional form of the stated model. Additionally, explicit solutions to this model are obtained. These solutions can be used to understand the system's dynamic properties better.

Outline of this work: Conversion to the ordinary differential form of the fractional TMNNV equation is presented in Section 2. Section 3 explains conformable fractional derivatives. In Section 4, the bifurcation analysis of the mentioned model is discussed. Section 5 determines the explicit solution

by bifurcation analysis and plotting the 3-D and 2-D graph solutions. In Section 6, some specific figures illustrate quasi-periodic and chaotic behavior with multistability. Finally, conclusions are drawn in Section 7.

The novelty of this paper is that the bifurcation, finding the outcome, phase portraits, and multistability of the suggested model are not described by any other investigator before.

2. Construction of the ordinary differential form of the TMNNV model

The (2+1)-dimensional TMNNV equation can be written in the next form [41]:

$$w_{tt} - p^2 w_{xx} - p^2 w_{yy} + \nu\left(\frac{\partial}{\partial t} - \gamma_1 p\frac{\partial}{\partial x} - \gamma_2 p\frac{\partial}{\partial y}\right)(w\int w\,dy)_x + \rho\left(\frac{\partial}{\partial t} - \alpha_1 p\frac{\partial}{\partial x} - \alpha_2 p\frac{\partial}{\partial y}\right)w_{xxx} = 0, \quad (1)$$

where $w = w(x, y, t)$ is the vector field with spatial variable $x, y,$ and temporal variable t. Here, γ_1 and γ_2 refer to the nonlinearity parameters, α_1 and α_2 denote the dispersion parameters, ν is the nonlinear interaction coefficient, ρ corresponds to the higher-order interaction coefficient, and p signifies the phase-velocity. Additionally, $|\alpha_1| \leq 1$, $|\alpha_2| \leq 1$, $|\gamma_1| \leq 1$, and $|\gamma_2| \leq 1$.

The time-fractional TMNNV equation Eq (1) can be written in the following way:

$$\frac{\partial^{2\beta} w}{\partial t^{2\beta}} - p^2 w_{xx} - p^2 w_{yy} + \nu\left(\frac{\partial^{\beta}}{\partial t^{\beta}} - \gamma_1 p\frac{\partial}{\partial x} - \gamma_2 p\frac{\partial}{\partial y}\right)(w\int w\,dy)_x + \rho\left(\frac{\partial^{\beta}}{\partial t^{\beta}} - \alpha_1 p\frac{\partial}{\partial x} - \alpha_2 p\frac{\partial}{\partial y}\right)w_{xxx} = 0, \quad (2)$$

where $\beta \in (0, 1]$. Consider a variable $\phi = \phi(x, y, t)$, which follows the next equation:

$$w = \phi_y. \quad (3)$$

Using Eq (3), the time fractional TMNNV equation (2) converts into

$$\frac{\partial^{2\beta+1}}{\partial t^{2\beta}\partial y}(\phi) - p^2\phi_{xxy} - p^2\phi_{yyy} + \nu\left(\frac{\partial^{\beta}}{\partial t^{\beta}} - \gamma_1 p\frac{\partial}{\partial x} - \gamma_2 p\frac{\partial}{\partial y}\right)(\phi_y\phi)_x + \rho\left(\frac{\partial^{\beta}}{\partial t^{\beta}} - \alpha_1 p\frac{\partial}{\partial x} - \alpha_2 p\frac{\partial}{\partial y}\right)\phi_{xxxy} = 0. \quad (4)$$

Now, Eq (4) needs to be convert into an ordinary differential equation with the relation as

$$\phi = R(\mu), \mu = cy + bx - \frac{at^{\beta}}{\beta}, \quad (5)$$

where $a, b,$ and c are arbitrary parameters. We assume that $\gamma_1 = \gamma_2 = \gamma$ and $\alpha_1 = \alpha_2 = \alpha$, then using Eqs (4) and (5), we obtain the resulting shortened ordinary differential form:

$$(a^2 - (b^2 + c^2)p^2)R(\mu) - \frac{1}{2}\nu b(a + (b + c)\gamma)R^2(\mu) - \rho b^3(\mathrm{a} + (b + c)\alpha)R''(\mu) = 0. \quad (6)$$

where $a, b, c, p, \nu, \rho, \gamma,$ and α are arbitrary parameters and " $'$ " represents the derivative over the independent variable μ.

3. Characteristics of fractional derivative

Let $f: [0, \infty] \to \mathbb{R}$ be a real function where $0 < \beta \leq 1$; with the conformable fractional

derivative of this function $f(\mathrm{q})$ at a point $q > 0$ takes the following form [41]:

$$\frac{\partial^{\beta}}{\partial q^{\beta}} f(\mathrm{q}) = \lim_{\epsilon \to 0} \frac{f\left(q + \epsilon q^{1-\beta}\right) - f(\mathrm{q})}{\epsilon}.$$

Assume that $f(q)$ and $g(q)$ are β-conformable differentiable functions while $q > 0$ and $0 < \beta \leq 1$. Some important characteristics of fractional derivatives are listed below where r is any constant and s and m are real constants.

(i) $\frac{\partial^{\beta}}{\partial q^{\beta}} q^{n} = n q^{n-\beta}, \ \forall n \in \mathbb{R}.$

(ii) $\frac{\partial^{\beta}}{\partial q^{\beta}} (\mathrm{r}) = 0.$

(iii) $\frac{\partial^{\beta}}{\partial q^{\beta}} sf(\mathrm{q}) = s \frac{\partial^{\beta}}{\partial q^{\beta}} f(q).$

(iv) $\frac{\partial^{\beta}}{\partial q^{\beta}} (sf(q) + mg(q)) = s \frac{\partial^{\beta}}{\partial q^{\beta}} f(q) + \mathrm{m} \frac{\partial^{\beta}}{\partial q^{\beta}} g(q).$

(v) $\frac{\partial^{\beta}}{\partial q^{\beta}} (g(q) f(q)) = g(q) \frac{\partial^{\beta}}{\partial q^{\beta}} f(q) + f(q) \frac{\partial^{\beta}}{\partial q^{\beta}} g(\mathrm{q}).$

(vi) $\frac{\partial^{\beta}}{\partial q^{\beta}} \left(\frac{f(q)}{g(q)}\right) = \frac{g(q) \frac{\partial^{\beta}}{\partial q^{\beta}} f(q) - f(q) \frac{\partial^{\beta}}{\partial q^{\beta}} g(q)}{g^{2}(q)}, \ g(q) \neq 0.$

4. Bifurcation analysis of the fractional TMNNV model

The bifurcation and phase representations [42,43] of the subsequent dynamical equation are discussed here. Let us assume that the differentiation of R over the variable μ is equal to Q; then a prototype differential system can be written from Eq (6) as follows:

$$\begin{cases} \frac{dR}{d\mu} = \mathrm{Q}, \\ \frac{dQ}{d\mu} = kR - lR^{2}, \end{cases} \tag{7}$$

which has the first integral

$$H(R, Q) = \frac{Q^{2}}{2} - \frac{k}{2} R^{2} + \frac{l}{3} R^{3} = h, \tag{8}$$

where $k = \frac{a^{2} - (b^{2} + c^{2}) p^{2}}{\rho b^{3} (\mathrm{a} + (b+c)\alpha)}$, $l = \frac{\nu b (a + (b+c)\gamma)}{2\rho b^{3} (\mathrm{a} + (b+c)\alpha)}$, and $H(R, Q)$ and h are the Hamiltonian function and constant, respectively.

Now, the bifurcation of the system (7) is discussed here with the arbitrary constants $a, b, c, p, \nu, \rho, \gamma$, and α. A smooth homoclinic orbit of Eq (7) is seen which rises from the smooth solitary waves in Eq (2) [44,45]. Consider that $\lim_{\mu \to -\infty} R(\mu) = d$ and $\lim_{\mu \to \infty} R(\mu) = e$ of the outcome $R\left(cy + bx - \frac{at^{\beta}}{\beta}\right) = R(\mu), (-\infty < \mu < \infty)$, then:

(i) When $d = e$, $R(\mu)$ is represented as a homoclinic orbit of Eq (7), which connects with a solitary wave outcome of Eq (2).

(ii) When $d \neq \mathrm{e}$, $R(\mu)$ is presumed to be a heteroclinic orbit of Eq (7), which connects with an antikink or a kink wave outcome of Eq (2).

Otherwise, a periodic orbit of Eq (7) connects with a periodic wave outcome of Eq (2). Therefore, we can easily analyze the probable phase portraits of Eq (7) with different constants $a, b, c, p, \nu, \rho, \gamma$, and α.

By inserting $R' = 0$ and $Q' = 0$ into Eq (7), then for $k \neq 0$, this system will deliver two equilibrium points $M_0(0,0)$ and $\mathrm{M}_1\left(\frac{k}{l}, 0\right)$. Moreover, at $k = 0$, the system (7) provides one equilibrium point $M(0,0)$. Assume that $B(R_M, Q_{\mathrm{M}})$ be the matrix of coefficients of the system (7) at equilibrium points $\mathrm{M}_j(j = 0, 1)$ and assume that $J(\mathrm{M}_j) = |B(R_M, Q_M)|$. Therefore, we have $J(M_0) = -k$, $J(M_1) = k$, $\mathrm{Trace}(B(M_0)) = 0$, $\mathrm{Trace}(B(M_1)) = 0$.

By exploring the bifurcations and the above outcomes, we can write the following categories:

Category-1: For $k > 0$, a saddle point and a center point can be seen of the nature at the points $M_0(0, 0)$ and $M_1\left(\frac{k}{l}, 0\right)$, respectively, while the equivalent phase portraits bifurcations of Eq (7) are imagined in Figure 1(a) and 1(b), respectively.

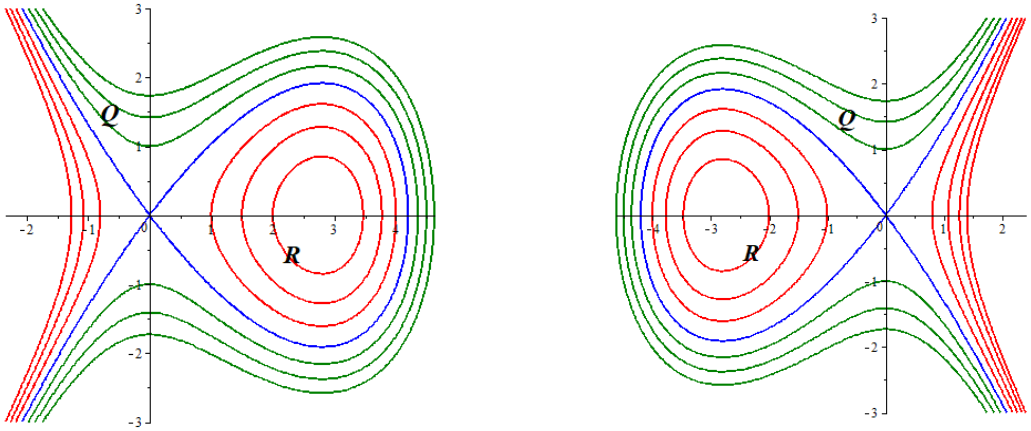

(a) (b)

Figure 1. The phase plot of the system (7) for (a) $k > 0$, $l > 0$, $\alpha = b = c = \gamma = \rho = p = \nu = 1$, $a = 3$ and (b) $k > 0$, $l < 0$, $\nu = -1$, $\alpha = b = c = \gamma = \rho = p = 1$, $a = 3$.

Category-2: For $k < 0$, a center point and a saddle point can be seen of the nature at the points $\mathrm{M}_0(0, 0)$ and $M_1\left(\frac{k}{l}, 0\right)$, respectively, while the equivalent phase portraits bifurcations of Eq (7) are drawn in Figure 2(a) and 2(b), respectively.

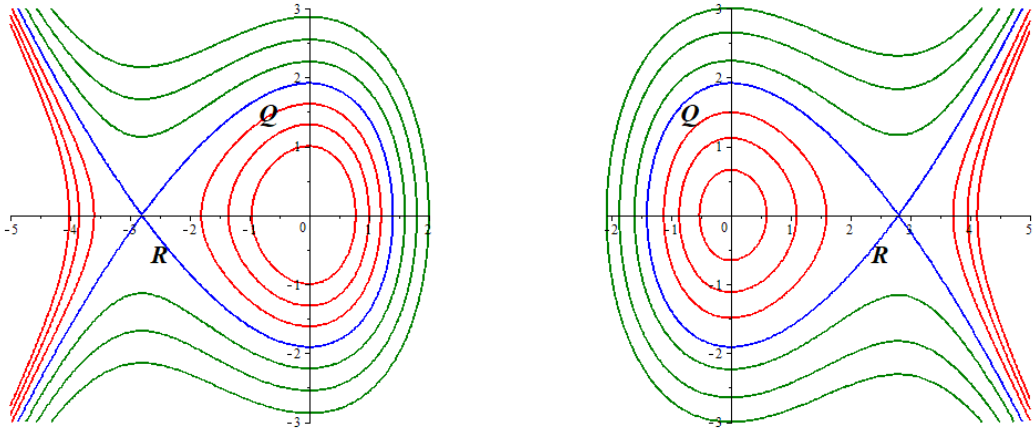

(a) (b)

Figure 2. The phase plot of the system (7) for (a) $k < 0,\ l > 0,\ \rho = \nu = -1,$ $\alpha = b = c = \gamma = p = 1,\ a = 3$ and (b) $k < 0,\ l < 0,\ \rho = -1,\ \alpha = b = c = \gamma = p = \nu = 1,\ a = 3.$

Category-3: For $k = 0,$ a cusp point can be seen of the nature at the points $M_0(0, 0)$, while the equivalent phase portraits bifurcations of Eq (7) are drawn in Figure 3(a) and 3(b), respectively.

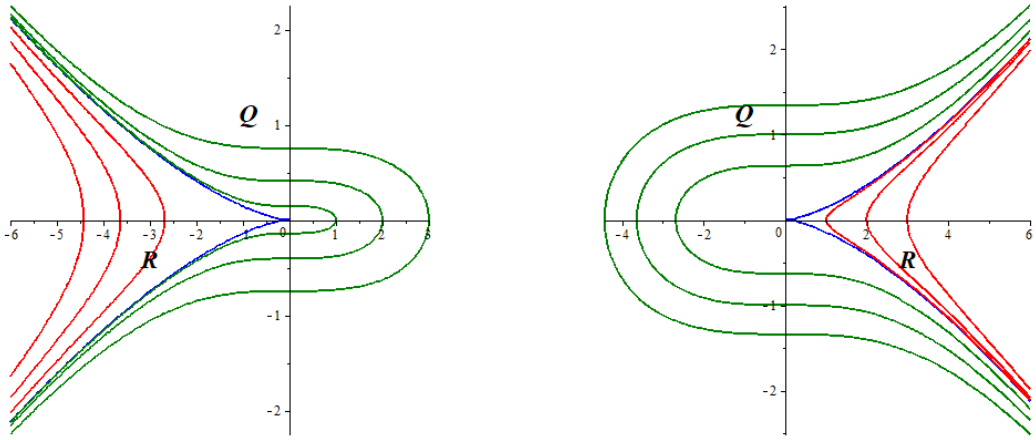

(a) (b)

Figure 3. The phase plot of system (7) for (a) $k = 0,\ l > 0,\ \alpha = \gamma = \rho = p = \nu = 1,\ c = 3,\ b = 4,\ a = 5$ and (b) $k = 0,\ l < 0,\ \rho = -1,\ \alpha = \gamma = p = \nu = 1,\ c = 3,\ b = 4,\ a = 5.$

A complete classification of equilibrium points is shown in Table 1.

Table 1. The Bifurcations Categories Summary.

Figure	State points		
	$(0,0)$	$(2.8,0)$	$(-2.8,0)$
1(a)	Unstable and saddle	Stable and center	-
1(b)	Unstable and saddle	-	Stable and center
2(a)	Stable and center	-	Unstable and saddle
2(b)	Stable and center	Unstable and saddle	-
3(a)	cusp point	-	-
3(b)	cusp point	-	-

5. Explicit solution for the proposed model

We aim to delve into the various explicit wave outcomes for the time fractional TMNNV model. For simplicity, the energy stage of the Hamiltonian is stated by taking $h_0 = H(0,0) = 0$ and $h_1 = H\left(\frac{k}{l}, 0\right) = -\frac{k^3}{6l^2}$.

5.1. Investigating category-1 in Section 4

5.1.1. Case-I

For $k > 0,\ l > 0,\ R(\mu)$ is expected to be a homoclinic orbit of Eq (7) at $M_0(0,0)$ defined by $H(R,Q) = h_0$, where Eq (2) provides a valley-type smooth solitary wave [42,43] outcome shown in Figure 1(a). By employing $H(R,Q) = h_0 = 0$ into Eq (8), we have

$$Q = \pm\sqrt{\frac{2l}{3}}R\sqrt{\frac{3k}{2l} - R}. \tag{9}$$

From the initial equation of the system (7) with Eqs (3), (5), and (9), we obtain

$$w = -\frac{3\mathrm{k}^{\frac{3}{2}}c}{2l}\mathrm{sech}^2\left(\frac{\sqrt{k}}{2}\ (\mu - \mu_0)\right)\tanh\left(\frac{\sqrt{k}}{2}\ (\mu - \mu_0)\right), \tag{10}$$

where $\mu = cy + bx - \frac{at^\beta}{\beta},\ k = \frac{a^2 - (b^2+c^2)p^2}{\rho b^3(\mathrm{a}+(b+c)\alpha)} > 0,\ l = \frac{\nu b(a+(b+c)\gamma)}{2\rho b^3(\mathrm{a}+(b+c)\alpha)} > 0,$ and μ_0 is an integrating constant.

A combo dark-bright bell wave [46,47] can be found in Figure 4 for the valley-type smooth solitary wave outcome Eq (10) with $\beta = 0.1, 0.4, 0.9;\ b = -1,\ \mu_0 = 0,\ a = c = p = \nu = \rho = 1,$ $\gamma = \alpha = 0.5$.

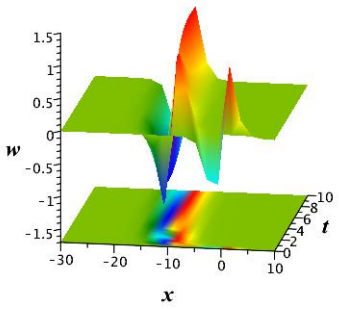

(a) 3D curve for $\beta = 0.1$

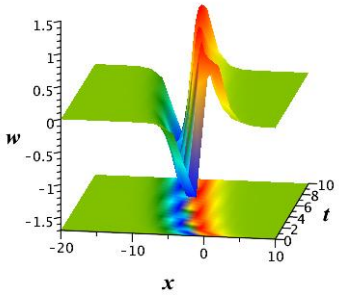

(b) 3D curve for $\beta = 0.5$

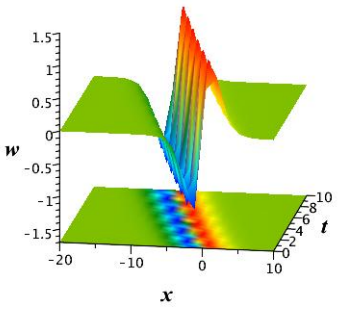

(c) 3D curve for $\beta = 0.9$

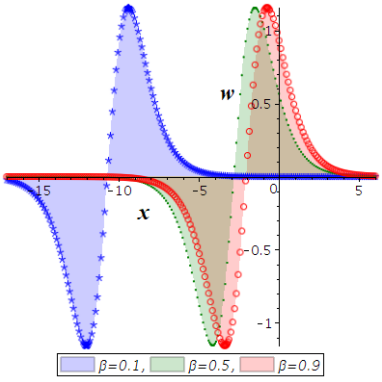

(d) 2D curve for $t = 2$ with $\beta = 0.1,\ 0.25$, and 0.9.

Figure 4. Visualization of Eq (10) for $b = -1,\ \mu_0 = 0,\ a = c = p = \nu = \rho = 1,\ \gamma = \alpha = 0.5$.

5.1.2. Case-II

For $k > 0, l < 0,\ R(\mu)$ is a homoclinic orbit of Eq (7) at $\mathrm{M}_0(0,0)$ defined by $H(R,Q) = h_0$, where Eq (2) provides a valley-type smooth solitary wave [42,43] outcome shown in Figure 1(b). By inserting $H(R,Q) = h_0 = 0$ into Eq (8), we obtain

$$Q = \pm\sqrt{\frac{2l}{3}}R\sqrt{\frac{3k}{2l} - R}. \tag{11}$$

From the initial equation of the system (7) with Eqs (3), (5), and (11), we obtain

$$w = -\frac{3\mathrm{k}^{\frac{3}{2}}c}{2l}\mathrm{sech}^2\left(\frac{\sqrt{k}}{2}(\mu - \mu_0)\right)\tanh\left(\frac{\sqrt{k}}{2}(\mu - \mu_0)\right), \tag{12}$$

where $\mu = cy + bx - \frac{at^\beta}{\beta}$, $k = \frac{a^2 - (b^2+c^2)p^2}{\rho b^3(\mathrm{a}+(b+c)\alpha)} > 0$, $l = \frac{\nu b(a+(b+c)\gamma)}{2\rho b^3(\mathrm{a}+(b+c)\alpha)} < 0$, and μ_0 is an integrating constant.

A combo bright-dark bell wave [42,43] can be found in Figure 5 for the valley-type smooth

solitary wave outcome equation (12) with $\beta = 0.1, 0.4, 0.9;\ b = v = -1,\ \mu_0 = 0,\ a = c = p = \rho = \gamma = 1,\ \alpha = 0.5$.

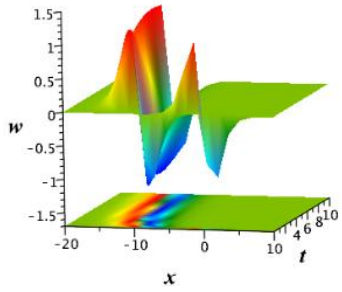

(a) 3D curve for $\beta = 0.1$

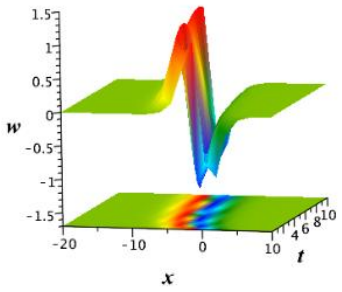

(b) 3D curve for $\beta = 0.4$

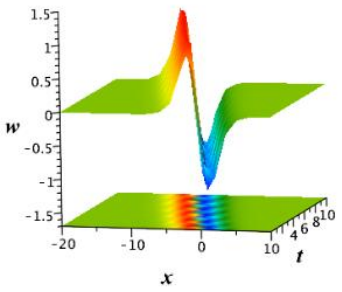

(c) 3D curve for $\beta = 0.9$

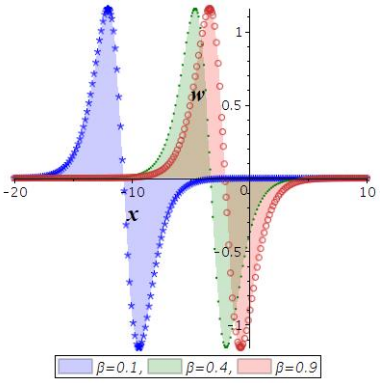

(d) 2D curve for $t = 2$ with $\beta = 0.1,\ 0.25$, and 0.9.

Figure 5. Visualization of Eq (12) for $b = v = -1,\ \mu_0 = 0,\ a = c = p = \rho = \gamma = 1,\ \alpha = 0.5$.

5.1.3. Case-III

For $k > 0,\ l > 0$ or $k > 0,\ l < 0$, Eq (2) provides a family of smooth periodic wave outcomes defined by $H(R, Q) = h,\ h \in (h_1, 0)$ (shown in Figure 1(a) and 1(b)).

For $k > 0,\ l > 0$, the expression of the closed domain of the system (7) is written below and displayed in Figure 1(a):

$$Q = \pm\sqrt{\frac{2l}{3}}\sqrt{(R - R_1)(R_2 - R)(R_3 - R)}, \tag{13}$$

where $(R_1, 0)$, $(R_2, 0)$, and $(R_3, 0)$ are the intersecting points of the graph defined by $H(R, Q) = h$, $h \in (h_1, 0)$ on the R-axis and holds the condition $R_1 < R < R_2 < \mathrm{R}_3$. From the initial equation of the system (7) with Eqs (3), (5), and (13), we obtain the formula of the periodic outcome as follows [48]:

$$w = \frac{c}{3}(R_2 - R_1)\sqrt{6l\big((R_3 - R_1)sn\left(\sqrt{\frac{l(R_3 - R_1)}{6}}(\mu - \mu_0), \sqrt{\frac{R_2 - R_1}{R_3 - R_1}}\right)}$$
$$cn\left(\sqrt{\frac{l(R_3-R_1)}{6}}(\mu - \mu_0), \sqrt{\frac{R_2-R_1}{R_3-R_1}}\right) dn\left(\sqrt{\frac{l(R_3-R_1)}{6}}(\mu - \mu_0), \sqrt{\frac{R_2-R_1}{R_3-R_1}}\right), \quad (14)$$

where $\mu = cy + bx - \frac{at^\beta}{\beta}$, $k = \frac{a^2-(b^2+c^2)p^2}{\rho b^3(a+(b+c)\alpha)} > 0$, $l = \frac{\nu b(a+(b+c)\gamma)}{2\rho b^3(a+(b+c)\alpha)} > 0$, and μ_0 is an integrating constant.

Periodic wave can be found in Figure 6 for the periodic wave outcome equation (14) with $\beta = 0.1, 0.6, 0.9$; $b = R_1 = -1$, $\mu_0 = 0$, $a = c = p = \nu = \rho = 1$, $\gamma = \alpha = 1$, $R_2 = 2$, $R_3 = 3$.

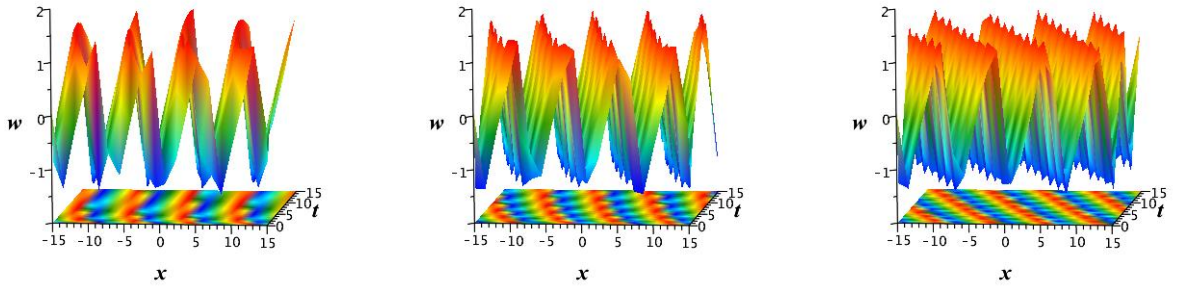

(a) 3D curve for $\beta = 0.1$ (b) 3D curve for $\beta = 0.6$ (c) 3D curve for $\beta = 0.9$

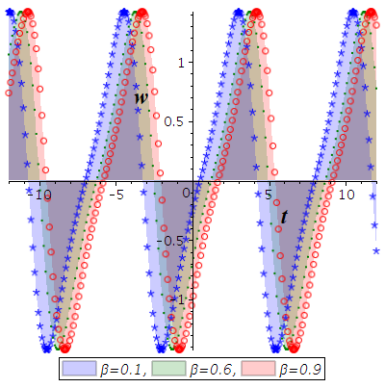

(d) 2D curve for $t = 2$ with $\beta = 0.1,\ 0.25$, and 0.9.

Figure 6. Visualization of Eq (14) for $b = R_1 = -1$, $\mu_0 = 0$, $a = c = p = \nu = \rho = \gamma = \alpha = 1$, $R_2 = 2$, $R_3 = 3$.

For $k > 0, l < 0$, a similar study can be found in Figure 1(b). Assume that $(R_4, 0)$, $(R_5, 0)$, and $(R_6, 0)$ are the touching points of the graph defined by $H(R, Q) = h, h \in (h_1, 0)$ on the R-axis and holds the condition $R_4 < R < R_5 < R_6$. We obtain the formula of the periodic outcome as follows [49]:

$$w = \frac{-1}{3((R_6 - R_5)\, sn^2\left(\frac{1}{6}\sqrt{6}\left(\sqrt{l(R_4 - R_6)}\left(cy + bx - \frac{at^\beta}{\beta}\right)\right), \sqrt{\frac{R_6 - R_5}{R_6 - R_4}}\right) + R_4 - R_6\Big)^2}$$

$$\left(\left(R_4(R_6 - R_4) - R_5(R_6 - R_4)\right)(R_6 - R_5)\, c\sqrt{6l(R_4 - R_6)}\; sn\left(\sqrt{\frac{l(R_4 - R_6)}{6}}(\mu - \mu_0), \sqrt{\frac{R_6 - R_5}{R_6 - R_4}}\right) cn\left(\sqrt{\frac{l(R_4 - R_6)}{6}}(\mu - \mu_0), \sqrt{\frac{R_6 - R_5}{R_6 - R_4}}\right) dn\left(\sqrt{\frac{l(R_4 - R_6)}{6}}(\mu - \mu_0), \sqrt{\frac{R_6 - R_5}{R_6 - R_4}}\right)\right), \quad (15)$$

where $\mu = cy + bx - \frac{at^\beta}{\beta}$, $k = \frac{a^2 - (b^2 + c^2)p^2}{\rho b^3(\mathrm{a} + (b+c)\alpha)} > 0$, $l = \frac{\nu b(a + (b+c)\gamma)}{2\rho b^3(\mathrm{a} + (b+c)\alpha)} < 0$, and μ_0 is an integrating constant.

A periodic wave pattern can be found for the outcome equation (15), which is almost like the periodic wave of the outcome equation (14).

5.2. Investigating category-2 in Section 4

5.2.1. Case-I

For $k < 0,\ l > 0,\ R(\mu)$ is expected to be a homoclinic orbit of Eq (7) at the stable point $M_1\left(\frac{k}{l}, 0\right)$ defined by $H(R, Q) = h_1$, and Eq (2) provides a valley-type smooth solitary wave [44,45] outcome shown in Figure 2(a). By substituting $H(R, Q) = h_1$ into Eq (8), we have

$$Q^2 = \frac{2l}{3}\left(R - \frac{k}{l}\right)^2\left(-R - \frac{k}{2l}\right). \quad (16)$$

From the initial equation of the system (7), with Eqs (3), (5), and (16), we obtain the following solution, which is like that shown in Figure 4.

$$w = \frac{3kc}{l}\sqrt{\frac{-k}{4}}\,\mathrm{sech}^2\left(\sqrt{\frac{-k}{4}}(\mu - \mu_0)\right)\tanh\left(\sqrt{\frac{-k}{4}}(\mu - \mu_0)\right), \quad (17)$$

where $\mu = cy + bx - \frac{at^\beta}{\beta}$, $k = \frac{a^2 - (b^2 + c^2)p^2}{\rho b^3(\mathrm{a} + (b+c)\alpha)} < 0$, $l = \frac{\nu b(a + (b+c)\gamma)}{2\rho b^3(\mathrm{a} + (b+c)\alpha)} > 0$, and μ_0 is an integrating constant.

5.2.2. Case-II

For $k < 0, l < 0,\ R(\mu)$ is supposed to be a homoclinic orbit of Eq (7) at the stable point $M_1\left(\frac{k}{l}, 0\right)$ is defined by $H(R, Q) = h_1$, and Eq (2) provides a valley-type smooth solitary wave outcome shown in Figure 2(b). By taking $H(R, Q) = h_1$ into Eq (8), we have

$$Q^2 = \frac{2l}{3}\left(R - \frac{k}{l}\right)^2 \left(-R - \frac{k}{2l}\right). \tag{18}$$

From the initial equation of the system (7) with Eqs (3), (5), and (18), we obtain the following solution which is like that shown in Figure 4.

$$w = \frac{3kc}{l}\sqrt{\frac{-k}{4}}\ \mathrm{sech}^2\left(\sqrt{\frac{-k}{4}}(\mu - \mu_0)\right)\tanh\left(\sqrt{\frac{-k}{4}}(\mu - \mu_0)\right), \tag{19}$$

where $\mu = cy + bx - \frac{at^\beta}{\beta}$, $k = \frac{a^2 - (b^2+c^2)p^2}{\rho b^3(\mathrm{a}+(b+c)\alpha)} < 0$, $l = \frac{\nu b(a+(b+c)\gamma)}{2\rho b^3(\mathrm{a}+(b+c)\alpha)} < 0$, and μ_0 is an integrating constant.

5.2.3. Case-III

For $k < 0, l > 0$ or $k < 0, l < 0$, Eq (2) provides a family of smooth periodic wave outcomes defined by $H(R,Q) = h, h \in (0, h_1)$, drawn in Figure 2(a) and 2(b), respectively. In addition, this periodic outcome is identical to the outcomes in Eqs (14) and (15).

5.3. Investigating category-3 in Section 4

5.3.1. Case-I

For $k = 0,\ l > 0,\ R(\mu)$ is assumed to be an unrestricted orbit of Eq (7) at $\mathrm{M}_0(0,0)$ defined by $H(R,Q) = h_0$, and Eq (2) provides a soliton solution shown in Figure 3(a). By inserting $H(R,Q) = h_0 = 0$ into Eq (8), we have

$$Q^2 = \frac{-2l}{3}R^3. \tag{20}$$

From the initial equation of the system (7) with Eqs (3), (5), and (20), we obtain the following soliton outcome:

$$w = \frac{12c}{l(\mu - \mu_0)^3}, \tag{21}$$

where $\mu = cy + bx - \frac{at^\beta}{\beta}$, $l = \frac{\nu b(a+(b+c)\gamma)}{2\rho b^3(\mathrm{a}+(b+c)\alpha)} > 0$, and μ_0 is an integrating constant.

A combo bright-dark bell wave with singularity can be found in Figure 7 for the soliton solution equation (21) with $\beta = 0.1, 0.25, 0.9;\ \mu_0 = 0,\ a = b = c = \nu = \rho = 1,\ p = \frac{1}{\sqrt{2}},\ \gamma = 1,\ \alpha = 0.5$.

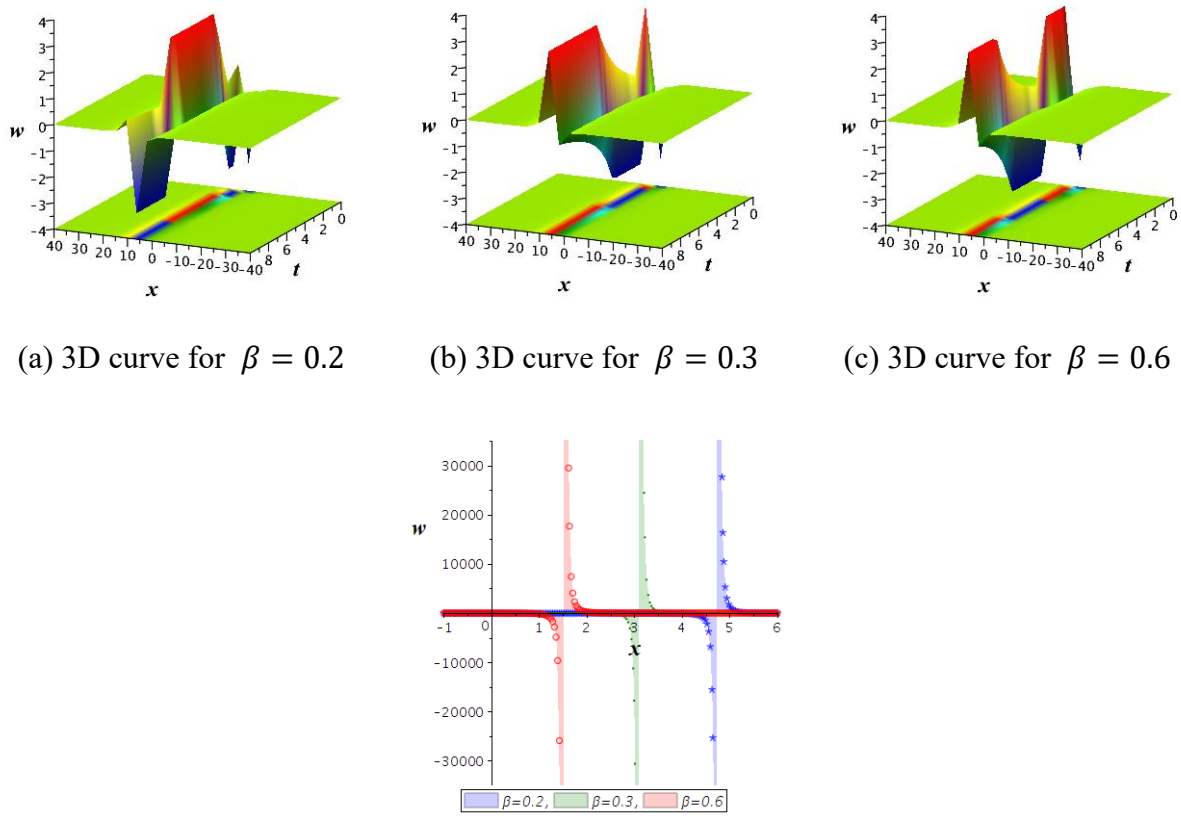

(a) 3D curve for $\beta = 0.2$ (b) 3D curve for $\beta = 0.3$ (c) 3D curve for $\beta = 0.6$

(d) 2D curve for $t = 2$ with $\beta = 0.2,\ 0.3$, and 0.6.

Figure 7. Visualization of Eq (21) for $\mu_0 = 0,\ a = b = c = \nu = \rho = 1,\ p = \frac{1}{\sqrt{2}},\ \gamma = 1,\ \alpha = 0.5$.

5.3.2. Case-II

For $k = 0,\ l < 0,\ R(\mu)$ is an unrestricted orbit of Eq (7) at $\mathrm{M}_0(0,0)$ defined by $H(R,Q) = h_0$, and Eq (2) provides a similar soliton solution shown in Figure 3(b). By substituting $H(R,Q) = h_0 = 0$ into Eq (8), we have

$$Q^2 = \frac{-2l}{3}R^3. \tag{22}$$

From the initial equation of the system (7) with Eqs (3), (5), and (22), we obtain the following soliton outcome which has a similar nature as shown in Figure 7:

$$w = \frac{12c}{l(\mu-\mu_0)^3}, \tag{23}$$

where $\mu = cy + bx - \frac{at^\beta}{\beta},\ l = \frac{\nu b(a+(b+c)\gamma)}{2\rho b^3(a+(b+c)\alpha)} < 0$, and μ_0 is an integrating constant.

6. Quasi-periodic and chaotic behaviors

Nonlinear models can exhibit chaotic behavior [50] when they experience bifurcations, leading to various dynamic properties. We saw in the previous section that the planar dynamical structure equation (7) does not exhibit chaotic properties, but it does when an external disturbance is added. Accordingly, for the dynamical system (7), perturbation takes the following shape:

$$\begin{cases} \frac{dR}{d\mu} = \mathrm{Q}, \\ \frac{dQ}{d\mu} = \left(\frac{a^2-(b^2+c^2)p^2}{\rho b^3(\mathrm{a}+(b+c)\alpha)}\right)R - \left(\frac{\nu b(a+(b+c)\gamma)}{2\rho b^3(\mathrm{a}+(b+c)\alpha)}\right)R^2 + F(\mu), \end{cases} \tag{24}$$

with perturbed term $F(\mu)$. In the context of phase portraits and multistability [49], quasi-periodic and chaotic behavior can be explored by considering the following three types of perturbation terms with diverse parameters. It is noted that chaotic waves demonstrate irregular, non-repeating structures and are highly sensitive to initial values. On the other hand, quasi-periodic waves frequently occur in coupled oscillators or systems with several degrees of freedom and have intricate but predictable structures that are not exactly repeatable. Some remarkable graphical representations, such as 3D phase portraits, 2D phase portraits, Poincaré plots, and time series plots, will be included to reach our destinations. Wave structures like these can be found in many natural phenomena, such as ocean waves, climate models, optics, telecommunications, plasma physics, and biological rhythms.

(i) **Trigonometric function:** Let $F(\mu) = 1.5\cos(3.9\,\mu)$, then the phase portrait and multistability of Eq (24) are exposed in Figures 8 and 11, respectively, for $\alpha = 1,\ \rho = 4,\ \gamma = 2,\ p = 4,\ a = 1,\ b = 0.5,\ c = 0.5$, and $\nu = 2$. Figure 8 shows that the system is chaotic, as evidenced by its irregular behavior and absence of regular patterns. Figure 11 shows that the system follows chaotic patterns due to its sensitivity to initial values.

(ii) **Gaussian function:** Let $F(\mu) = 3.5\,e^{\frac{-(0.12\mu)^2}{2}}$, then the phase portrait and multistability of Eq (24) are exposed in Figures 9 and 12, respectively, for parameters $\alpha = 1,\ \rho = 4,\ \gamma = 2,\ p = 4,\ a = 1,\ b = 0.5,\ c = 0.5,$ and $\nu = 2$. Figures 9 and 12 represent quasi-periodic structures, evidenced by the periodic irregularity of the wave.

(iii) **Hyperbolic function:** Let $F(\mu) = 1.4\cosh(0.04\mu)$, then the phase portrait and multistability of Eq (24) are exposed in Figures 10 and 13, respectively for parameters $\alpha = 1,\ \rho = 4,\ \gamma = 2,\ p = 4,\ a = 1,\ b = 0.5,\ c = 0.5,$ and $\nu = 2$. Figures 10 and 13 represent quasi-periodic structures, as evidenced by the wave's periodic irregularity.

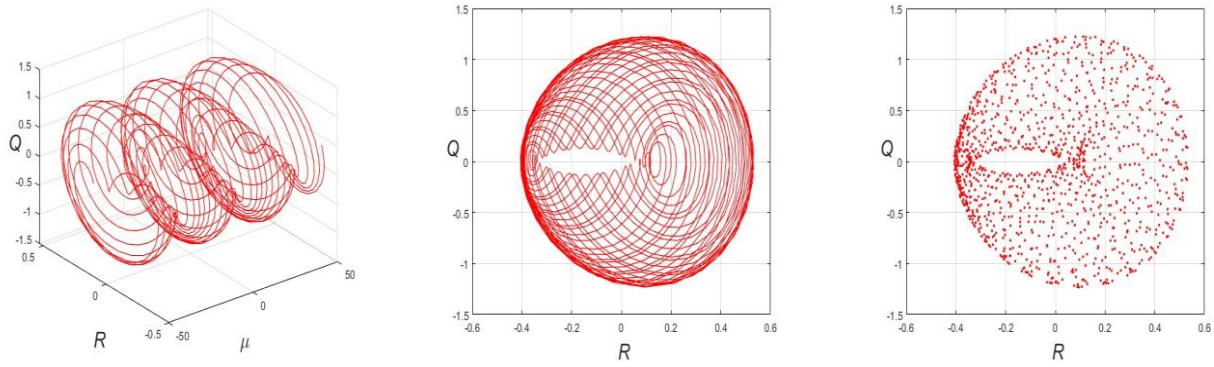

(a) 3D phase portrait (b) 2D phase portrait (c) Poincaré plot

Figure 8. Outlook of the perturbation equation (24) for $F(\mu) = 1.5\cos(3.9\,\mu)$ with initial value $\big(R(0), Q(0)\big) = (0.1, 0.1)$.

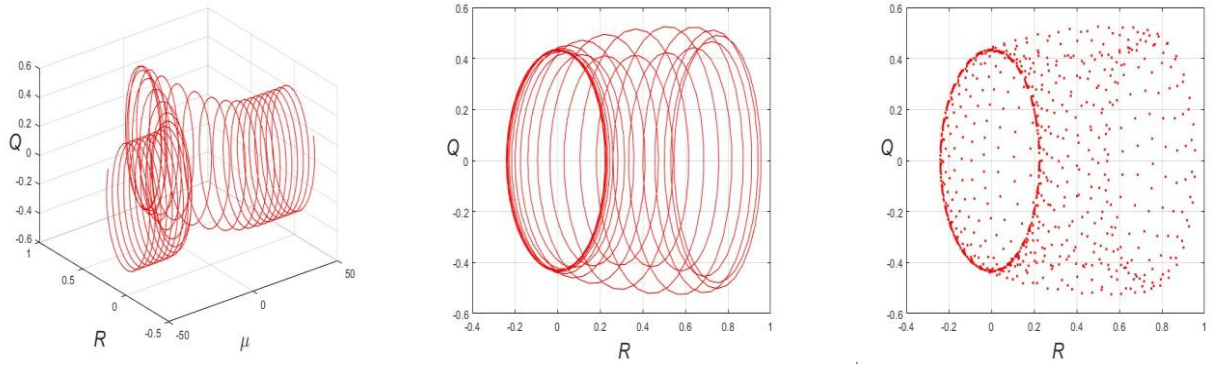

(a) 3D phase portrait (b) 2D phase portrait (c) Poincaré plot

Figure 9. Outlook of the perturbation equation (24) for $F(\mu) = 3.5\,e^{\frac{-(0.12\mu)^2}{2}}$ with initial value $\big(R(0), Q(0)\big) = (0.2, 0.2)$.

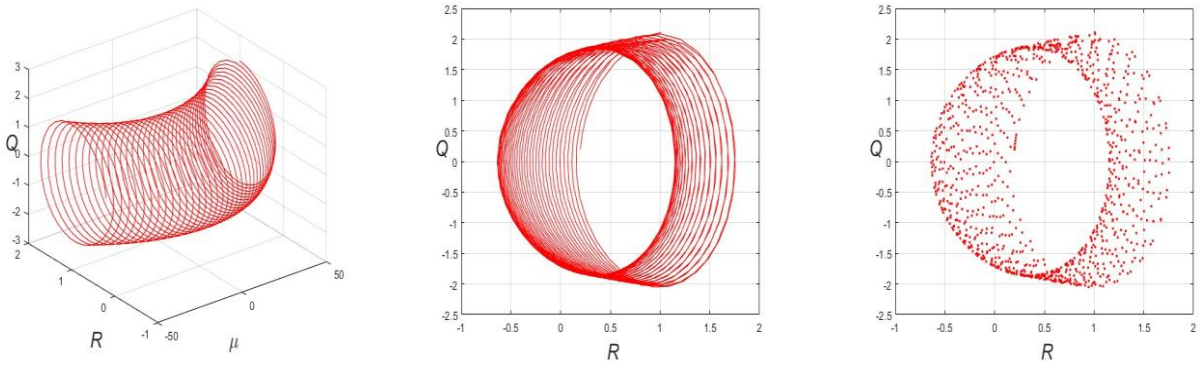

(a) 3D phase portrait (b) 2D phase portrait (c) Poincaré plot

Figure 10. Outlook of the perturbation equation (24) for $F(\mu) = 1.4\cosh(0.04\mu)$ with initial value $\big(R(0), Q(0)\big) = (0.2, 0.2)$.

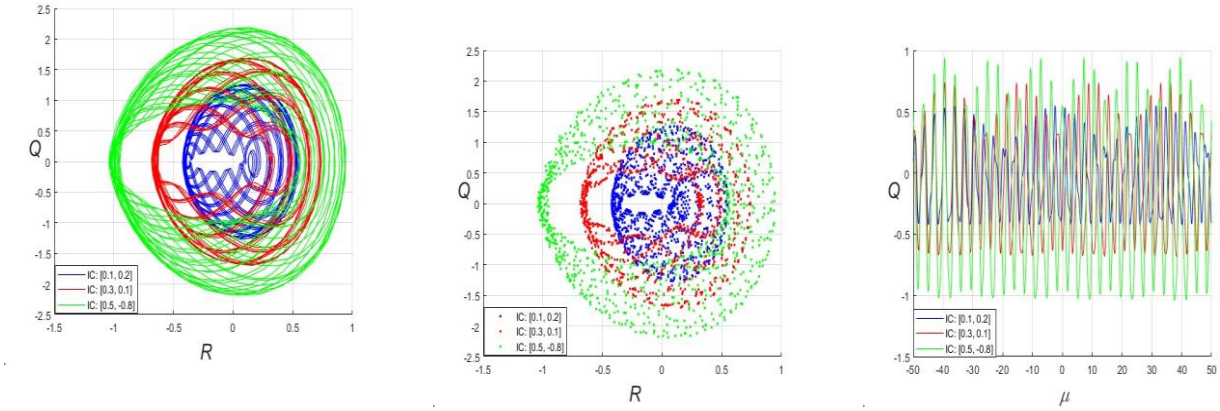

(a) 2D phase portrait (b) Poincaré plot (c) time series plot

Figure 11. Multistability of the perturbation equation (24) for $(\mu) = 1.5\cos(3.9\,\mu)$.

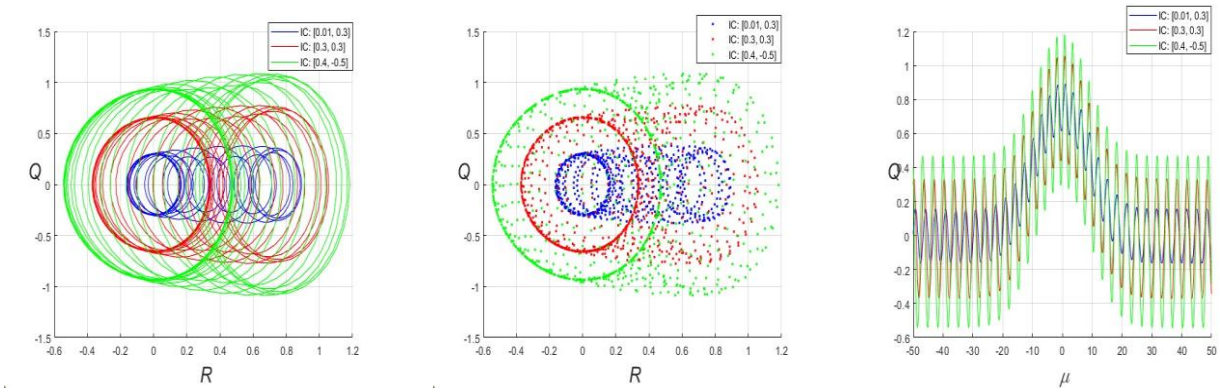

(a) 2D phase portrait (b) Poincaré plot (c) time series plot

Figure 12. Multistability of the perturbation equation (24) for $F(\mu) = 3.5\,e^{\frac{-(0.12\mu)^2}{2}}$.

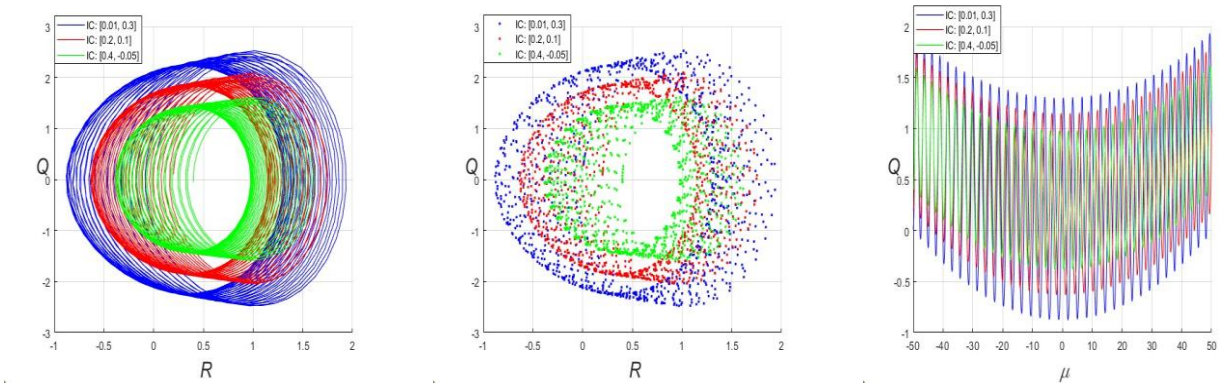

(a) 2D phase portrait (b) Poincaré plot (c) time series plot

Figure 13. Multistability of the perturbation equation (24) for $F(\mu) = 1.4\cosh(0.04\mu)$.

7. Conclusions

We apply bifurcation theory to the TMNNV model for the first time to uncover bifurcations, discrete solutions, phase portraits, and multistability under different parameters. 3D with density and 2D plots are used to identify and visualize unique wave patterns, such as combined bright-dark and dark-bright bell waves, periodic waves, and bright solitons. Additionally, quasi-periodic and chaotic behaviors are studied, along with multistability, showing how they are strongly dependent on initial conditions and parameter settings. The findings shed light on the dynamics of these nonlinear systems, providing valuable insights into their behavior. Based on this analysis and graphical representation, future physical experiments or observations can be conducted to validate these predicted complex dynamics and their practical applications.

Author contributions

Noor Alam: Formal analysis, Software; Mohammad Safi Ullah: Validation, Methodology; Jalil Manafian: Investigation, Writing–review & editing; Khaled H. Mahmoud: Software, Writing–review & editing; A. SA. Alsubaie: Formal analysis, Writing–review & editing; Hamdy M. Ahmed: Supervision, Software; Karim K. Ahmed: Resources, Writing–review & editing; Soliman Alkhatib: Mathematical analysis, Writing–review & editing. All authors have read and agreed to the published version of the manuscript.

Use of Generative-AI tools declaration

The authors declare they have used Artificial Intelligence (AI) tools in the creation of this article.

Acknowledgments

The authors extend their appreciation to Taif University, Saudi Arabia, for supporting this work through project number (TU-DSPP-2024-106).

Funding

This research was funded by Taif University, Saudi Arabia, Project No. (TU-DSPP-2024-106).

Conflict of interest

The authors declare that they have no competing interests.

References

1. A. S. Joglekar, A. G. R. Thomas, Unsupervised discovery of nonlinear plasma physics using differentiable kinetic simulations, *J. Plasma Phys.*, **88** (2022), 905880608. https://doi.org/10.1017/S0022377822000939
2. O. A. Ilhan, J. Manafian, M. Lakestani, G. Singh, Some novel optical solutions to the perturbed nonlinear Schrödinger model arising in nano-fibers mechanical systems, *Mod. Phys. Lett. B*, **36** (2022), 2150551. https://doi.org/10.1142/S0217984921505515
3. N. Alam, S. Poddar, M. E. Karim, M. S. Hasan, G. Lorenzini, Transient MHD radiative fluid flow over an inclined porous plate with thermal and mass diffusion: an EFDM numerical approach, *Math. Model. Eng. Probl.*, **8** (2021), 739–749. https://doi.org/10.18280/MMEP.080508
4. N. Zhao, J. Manafian, O.A. Ilhan, G. Singh, R. Zulfugarova, Abundant interaction between lump and *k*-kink, periodic and other analytical solutions for the (3+1)-D Burger system by bilinear analysis, *Int. J. Mod. Phys. B*, **35** (2021), 2150173. https://doi.org/10.1142/S0217979221501733
5. W. X. Ma, Soliton hierarchies and soliton solutions of type $(-\lambda^*,-\lambda)$ reduced nonlocal nonlinear Schrödinger equations of arbitrary even order, *Partial Differ. Equ. Appl. Math.*, **7** (2023), 100515. https://doi.org/10.1016/J.PADIFF.2023.100515
6. S. Duran, A. Yokus, G. Kilinc, A study on solitary wave solutions for the Zoomeron equation supported by two-dimensional dynamics, *Phys. Scr.*, **98** (2023), 125265. https://doi.org/10.1088/1402-4896/AD0C3C
7. M. Z. Baber, N. Ahmed, C. J. Xu, M. S. Iqbal, T. A. Sulaiman, A computational scheme and its comparison with optical soliton solutions for the stochastic Chen-Lee-Liu equation with sensitivity analysis, *Mod. Phys. Lett. B*, **39** (2025), 2450376. https://doi.org/10.1142/S0217984924503767
8. X. Shi, U. Ishtiaq, M. Din, M. Akram, Fractals of interpolative Kannan mappings, *Fractal Fract.*, **8** (2024), 493.
9. H. X. Zhang, J. Manafian, G. Singh, O. A. Ilhan, A. O. Zekiy, N-lump and interaction solutions of localized waves to the (2+1)-dimensional generalized KP equation, *Results Phys.,* **25** (2021), 104168. https://doi.org/10.1016/J.RINP.2021.104168
10. N. Ahmed, M. Z. Baber, M. S. Iqbal, A. Akgül, M. Rafiq, A. Raza, et al., Investigation of soliton structures for dispersion, dissipation, and reaction time-fractional KdV-burgers-Fisher equation with the noise effect, *Int. J. Mod. Simul.*, 2024, 1–17. https://doi.org/10.1080/02286203.2024.2318805
11. M. Alquran, M. Ali, H. Jadallah, New topological and non-topological unidirectional-wave solutions for the modified-mixed KdV equation and bidirectional-waves solutions for the Benjamin Ono equation using recent techniques, *J. Ocean Eng. Sci.*, **7** (2022), 163–169. https://doi.org/10.1016/J.JOES.2021.07.008

12. X. Y. Gao, In plasma physics and fluid dynamics: symbolic computation on a (2+1)-dimensional variable-coefficient Sawada-Kotera system, *Appl. Math. Lett.*, **159** (2025), 109262. https://doi.org/10.1016/j.aml.2024.109262
13. M. C. Zhang, X. Xie, J. Manafian, O. A. Ilhan, G. Singh, Characteristics of the new multiple rogue wave solutions to the fractional generalized CBS-BK equation, *J. Adv. Res.*, **38** (2022), 131–142. https://doi.org/10.1016/J.JARE.2021.09.015
14. W. X. Ma, A novel kind of reduced integrable matrix mKdV equations and their binary Darboux transformations, *Mod. Phys. Lett. B*, **36** (2022), 2250094. https://doi.org/10.1142/S0217984922500944
15. A. H. Arnous, Q. Zhou, A. Biswas, P. Guggilla, S. Khan, Y. Yıldırım, et al., Optical solitons in fiber Bragg gratings with cubic-quartic dispersive reflectivity by enhanced Kudryashov's approach, *Phys. Lett. A*, **422** (2022), 127797. https://doi.org/10.1016/J.PHYSLETA.2021.127797
16. S. T. Mohyud-Din, A. Irshad, N. Ahmed, U. Khan, Exact solutions of $(3 + 1)$-dimensional generalized KP equation arising in physics, *Results Phys.*, **7** (2017), 3901–3909. https://doi.org/10.1016/J.RINP.2017.10.007
17. I. Onder, A. Secer, M. Ozisik, M. Bayram, On the optical soliton solutions of Kundu-Mukherjee-Naskar equation via two different analytical methods, *Optik*, **257** (2022), 168761. https://doi.org/10.1016/J.IJLEO.2022.168761
18. Y. Xu, Z. Xie, J. Zhao, W. Li, P. Li, P. K. Wong, Robust non-fragile finite frequency H_∞ control for uncertain active suspension systems with time-delay using T-S fuzzy approach, *J. Franklin Inst.*, **358** (2021), 4209–4238. https://doi.org/10.1016/j.jfranklin.2021.03.019
19. D. A. Juraev, Y. S. Gasimov, On the regularization Cauchy problem for matrix factorizations of the Helmholtz equation in a multidimensional bounded domain, *Azerbaijan J. Math.*, **12** (2022), 142–161.
20. L. Wang, G. Y. Liu, G. L. Wang, K. Zhang, M-PINN: A mesh-based physics-informed neural network for linear elastic problems in solid mechanics, *Int. J. Numer. Methods Eng.*, **125** (2024), e7444. https://doi.org/10.1002/nme.7444
21. M. A. Akbar, N. H. M. Ali, S. T. Mohyud-Din, The modified alternative (G'/G)-expansion method to nonlinear evolution equation: application to the (1+1)-dimensional Drinfel'd-Sokolov-Wilson equation, *SpringerPlus*, **2** (2013), 327. https://doi.org/10.1186/2193-1801-2-327
22. N. Alam, A. Akbar, M. S. Ullah, M. Mostafa, Dynamic waveforms of the new Hamiltonian amplitude model using three different analytic techniques, *Indian J. Phys.*, 2024, 1–8. https://doi.org/10.1007/s12648-024-03426-7
23. Y. H. Wu, T. L. Shen, A finite convergence criterion for the discounted optimal control of stochastic logical networks, *IEEE Trans. Automatic Control*, **63** (2018), 262–268. https://doi.org/10.1109/TAC.2017.2720730
24. A. Ghosh, S. Maitra, The first integral method and some nonlinear models, *Comput. Appl. Math.*, **40** (2021), 79. https://doi.org/10.1007/S40314-021-01470-1/METRICS
25. E. H. M. Zahran, M. M. A. Khater, Modified extended tanh-function method and its applications to the Bogoyavlenskii equation, *Appl. Math. Model.*, **40** (2016), 1769–1775. https://doi.org/10.1016/J.APM.2015.08.018
26. K. K. Ahmed, N. M. Badra, H. M. Ahmed, W. B. Rabie, Unveiling optical solitons and other solutions for fourth-order (2+1)-dimensional nonlinear Schrödinger equation by modified extended direct algebraic method, *J. Opt.*, 2024, 1–13. https://doi.org/10.1007/s12596-024-01690-8

27. W. Li, Z. Xie, P. K. Wong, X. Mei, J. Zhao, Adaptive-event-trigger-based fuzzy nonlinear lateral dynamic control for autonomous electric vehicles under insecure communication networks, *IEEE Trans. Indust. Electronics*, **68** (2021), 2447–2459.
28. X. H. Wu, Y. T. Gao, X. Yu, Dark-soliton asymptotics for a repulsive nonlinear system in a baroclinic flow, *Phys. Fluids*, **36** (2024), 056615. https://doi.org/10.1063/5.0213090
29. T. Y. Zhou, B. Tian, Y. Shen, X. T. Gao, Auto-Bäcklund transformations and soliton solutions on the nonzero background for a (3+1)-dimensional Korteweg-de Vries-Calogero-Bogoyavlenskii-Schif equation in a fluid, *Nonlinear Dyn.*, **111** (2023), 8647–8658. https://doi.org/10.1007/s11071-023-08260-w
30. K. K. Ahmed, H. M. Ahmed, N. M. Badra, M. Mirzazadeh, W. B. Rabie, M. Eslami, Diverse exact solutions to Davey-Stewartson model using modified extended mapping method, *Nonlinear Anal. Model. Control*, **29** (2024), 983–1002. https://doi.org/10.15388/namc.2024.29.36103
31. M. Alquran, I. Jaradat, Identifying combination of dark-bright binary-soliton and binary-periodic waves for a new two-mode model derived from the (2+1)-dimensional Nizhnik-Novikov-Veselov equation, *Mathematics*, **11** (2023), 1–9. https://doi.org/10.3390/MATH11040861
32. H. Jiang, S. M. Li, W. G. Wang, Moderate deviations for parameter estimation in the fractional Ornstein-Uhlenbeck processes with periodic mean, *Acta Math. Sin. English Ser.*, **40** (2024), 1308–1324. https://doi.org/10.1007/s10114-023-2157-z
33. F. Meng, A. Pang, X. Dong, C. Han, X. Sha, H_∞ optimal performance design of an unstable plant under bode integral constraint, *Complexity*, **2018** (2018), 4942906. https://doi.org/10.1155/2018/4942906
34. G. Y. Jia, J. X. Luo, C. Y. Cui, R. J. Kou, Y. L. Tian, M. Schubert, Valley quantum interference modulated by hyperbolic shear polaritons, *Phys. Rev. B*, **109** (2024), 155417. https://doi.org/10.1103/PhysRevB.109.155417
35. W. Xu, E. Aponte, P. Vasanthakumar, The property ($\omega\pi$) as a generalization of the a-Weyl theorem, *AIMS Math.*, **9** (2024), 25646–25658. https://doi.org/10.3934/math.20241253
36. L. P. Wan, D. Raveh, T. B. Yu, D. M. Zhao, O. Korotkova, Optical resonance with subwavelength spectral coherence switch in open-end cavity, *Sci. China Phys. Mech. Astron.*, **66** (2023), 274213. https://doi.org/10.1007/s11433-023-2097-9
37. Y. Kai, Z. X. Yin, On the Gaussian traveling wave solution to a special kind of Schrödinger equation with logarithmic nonlinearity, *Mod. Phys. Lett. B*, **36** (2022), 2150543. https://doi.org/10.1142/S0217984921505436
38. Y. Kai, S. Q. Chen, K. Zhang, Z. X. Yin, Exact solutions and dynamic properties of a nonlinear fourth-order time-fractional partial differential equation, *Waves Random Complex Media*, 2022, 1–12. https://doi.org/10.1080/17455030.2022.2044541
39. C. Y. Zhu, S. A. Idris, M. E. M. Abdalla, S. Rezapour, S. Shateyi, B. Gunay, Analytical study of nonlinear models using a modified Schrödinger's equation and logarithmic transformation, *Res. Phys.*, **55** (2023), 107183. https://doi.org/10.1016/j.rinp.2023.107183
40. S. J. Guo, A. Das, Cohomology and deformations of generalized Reynolds operators on Leibniz algebras, *Rocky Mountain J. Math.*, **54** (2024), 161–178. https://doi.org/10.1216/rmj.2024.54.161
41. R. Khalil, M. Al Horani, A. Yousef, M. Sababheh, A new definition of fractional derivative, *J. Comput. Appl. Math.*, **264** (2014), 65–70. https://doi.org/10.1016/J.CAM.2014.01.002

42. S. Uddin, S. Karim, F. S. Alshammari, H. O. Roshid, N. F. M. Noor, F. Hoque, et al., Bifurcation analysis of travelling waves and multi-rogue wave solutions for a nonlinear pseudo-parabolic model of visco-elastic Kelvin-Voigt fluid, *Math. Probl. Eng.*, **2022** (2022), 8227124. https://doi.org/10.1155/2022/8227124
43. Z. G. Liu, K. L. Zhang, M. Y. Li, Exact traveling wave solutions and bifurcation of a generalized (3+1)-dimensional time-fractional Camassa-Holm-Kadomtsev-Petviashvili equation, *J. Funct. Spaces*, **2020** (2020), 4532824. https://doi.org/10.1155/2020/4532824
44. D. H. Feng, J. B. Li, J. J. Jiao, Dynamical behavior of singular traveling waves of (n+1)-dimensional nonlinear Klein-Gordon equation, *Qual. Theory Dyn. Syst.*, **18** (2019), 265–287. https://doi.org/10.1007/s12346-018-0285-0
45. P. F. Byrd, M. D. Friedman, Reduction of algebraic integrands to Jacobian elliptic functions, In: *Handbook of elliptic integrals for engineers and scientists*, Berlin, Heidelberg: Springer, 1971, 42–161. https://doi.org/10.1007/978-3-642-65138-0_3
46. B. He, J. B. Li, Y. Long, W. G. Rui, Bifurcations of travelling wave solutions for a variant of Camassa-Holm equation, *Nonlinear Anal. Real World Appl.*, **9** (2008), 222–232. https://doi.org/10.1016/J.NONRWA.2006.10.001
47. Y. Q. Zhou, Q. Liu, Kink waves and their evolution of the RLW-Burgers equation, *Abst. Appl. Anal.*, **2012** (2012), 109235. https://doi.org/10.1155/2012/109235
48. I. Samir, K. K. Ahmed, H. M. Ahmed, H. Emadifar, W. B. Rabie, Extraction of newly soliton wave structure of generalized stochastic NLSE with standard Brownian motion, quintuple power law of nonlinearity and nonlinear chromatic dispersion, *Phys. Open*, **21** (2024), 100232. https://doi.org/10.1016/j.physo.2024.100232
49. M. S. Ullah, M. Z. Ali, H. O. Roshid, Bifurcation, chaos, and stability analysis to the second fractional WBBM model, *PLoS One*, **19** (2024), e0307565. https://doi.org/10.1371/journal.pone.0307565
50. M. S. Ullah, M. Z. Ali, H. O. Roshid, Bifurcation analysis and new waveforms to the first fractional WBBM equation, *Sci. Rep.*, **14** (2024), 11907. https://doi.org/10.1038/s41598-024-62754-0